The middle Jurassic–Early Cretaceous pillow and massive lava flows associated with pelagic sediments in the Ghaleh-Rigi area, southern east of Iran: age and geochemistry

Hojatollah Jahangiri[1], Saeed Saadat[2*], Seyed Ahmad Mazaheri[1], Mohammad Reza Heidarian Shahri[1], Mohammad Foudazi[3], Seyed Jafar Omrani[4]

[1] *Department of Geology, Ferdowsi University of Mashhad, Mashhad, Iran*

[2] *Department of Geology and Petroleum Engineering, Mashhad Branch, Islamic Azad University, Mashhad, Iran*

[3] *Department of Geology, Islamshar Branch, Islamic Azad University, Islamshahr, Iran*

[4] *Geological Survey and Mineral Exploration of Iran, Tehran, Iran*

**Corresponding author, e–mail: saeed.saadat@colorado.edu*

(*received: 19/03/2019 ; accepted: 11/12/2019*)

Abstract

The Ghaleh-Rigi complex is located in northern margin of the Sanandaj–Sirjan Zone (western Iran) and the southern part of the Central Iran Micro-continent block. The study area is covered by pillow and massive lava flows associated with micro gabbro and pelagic sediments including mudstone and radiolarian ribbon chert. Geochemical analysis indicates similar mantle source for magmatic rocks. These rocks show tholeiitic affinity with depletion in high-field strength elements (HFSEs) and light rare-earth elements (LREEs). They also show enrichment in large-ion lithophile elements (LILEs) in primitive mantle normalized multi-element diagrams. All samples show variable depletion in Th followed by depletion of HFSE and trace element concentrations and negative Nb anomaly (Th/Nb=0.23-035), which is a typical characteristic from magmas related to subduction zone. In addition, ratio of Y/Nb against Zr/Nb and Ce/Y against Zr/Nb and also REE flat patterns are similar to N-MORB-like source. These features suggest generation of magma in the back-arc basin. According to geochemical and petrogenesis studies, these rocks shows around 10% partial melting of a mixed spinel–garnet-bearing source composed of 50% PM and 50% MORB source. Based on bio-chronological investigation, the radiolarian cherts associated with volcanic rocks show Early Bajocian to Berriasian; Callovian- Valanginian; and Oxfordian- Valanginian ages**.**

Keywords: *Pillow Lava, Radiolarian Biostratigraphy, Early Middle Jurassic, Central Iran, Ghaleh-Rigi.*

Introduction

The paleotectonic history of Iran has characterized by the existence of numerous micro continental blocks, which has recorded the fragmentation of Gondwana-derived crustal segments in Permian time (Golonka, 2004; Robertson, 2007; Saccani *et al.,* 2012; Stampfli *et al.,* 2001). Due to the complex interaction between individual blocks and a severe lack of robust geochronological evidence, it has not been yet possible to fully resolve the regional geodynamic framework. Detailed knowledge about the existence and life span of oceanic basins surrounding individual continental segments plays a key role in understanding the geotectonic history that have been strongly affected by various stages of the Arabia–Eurasia collision and closing of different Tethyan oceanic basins (e.g. Marroni *et al.,* 2019). Many ophiolites in Iran are remnants of Neotethys ocean basins and belong to an ophiolite belt extending from Cyprus to Oman that marks an important segment of the Alpine–Himalayan orogeny (Dilek *et al*., 2019; Shafaii Moghadam & Stern, 2011; and references in Brocker *et al*., 2011). The Iranian ophiolites are part of Tethyan ophiolite belt extending from eastern Europe, through Mediterranean and middle east, to eastern Asia (Moores *et al*., 2000; Shojaat *et al.,* 2003; Zhang *et al.,* 2005; Shafaii Moghadam *et al.,* 2010; Shafaii Moghadam & Stern, 2011) (Fig. 1a). The ophiolites of Iran form two distinct groups based on their age and abundances, the less abundant ones are Paleozoic age (Weber-diefenbach *et al.*, 1986) along the paleo-Tethys suture, (Fig. 1) and the more abundant ones are Mesozoic ophiolites (Alavi, 1991; Arvin & Robinson, 1994). They have divided into three sub belts (Takin, 1972; Stocklin, 1968, 1974; McCall, 1997). The first one (i) ophiolites of the Zagros suture zone, including the Neyriz and Kermanshah ophiolites, which appear to be coeval with the Oman (Smail) ophiolites emplaced onto Arabian continental margin. The second (ii) un-fragmented ophiolites of the Makran accretionary prism, which includes Bande Zyarat, Dar Anar and Mokhtar Abad (southeast of Iran ophiolites). Lastly, the third (iii) ophiolites and colored mélanges that mark the boundaries of the Central Iran microplate including Shahar Babak Nain, Baft, Sabzavar, and Tchehel Kureh ophiolites (Fig.1b).

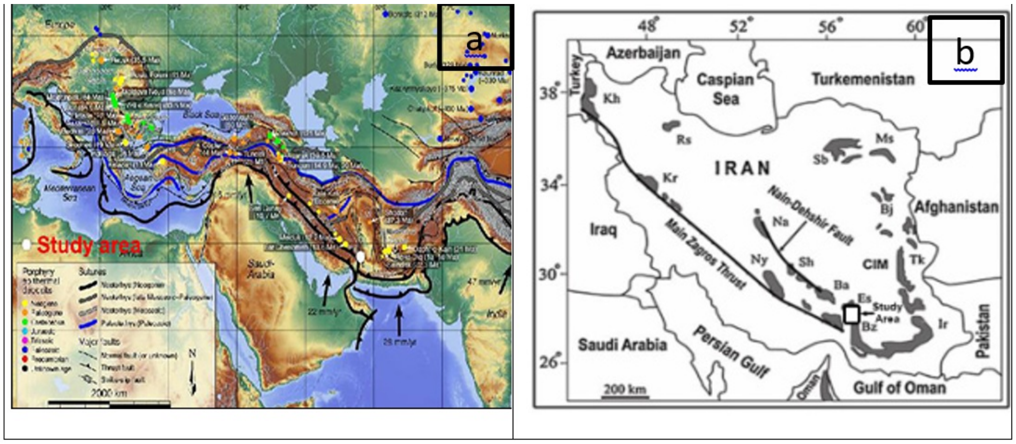

Figure 1. (a) Topographic relief map of the Alpine- Himalayan Tethyan organic belt, showing major structures, Tethyan suture (Richards, 2014) black line= Neotethys (Neogene), dark grey line= Neotethys (late Mesozoic-paleozoic), pale grey line= Neotethys (Mesozoic) blue line= paleotethys (Paleozoic), white vertical oral= study area (b) Distribution of different ophiolite complexes in Iran (Mehdipour Ghazi *et al.,* 2010). Kh: Khoy, Rs: Rasht, Kr: Kermanshah, Ny: Neyriz, Bz: Bande-Zyarat, Ir: Iranshahr, Es: Esfandagheh, Ba: Baft, Sh, Shahre-Babak, Na: Nain, Sb: Sabzevar, Ms: Mashhad, Bj: Birjand, Tk: Tchehel Kureh.

Throughout the world, in various tectonic settings, in the highest part of oceanic lithosphere, there are pillow and massive lava flows accompanied with pelagic sediment that belong to deep oceanic basin and often are associated with ophiolitic rocks and colored mélange complex. The presence and continuity pelagic sediment with pillow and massive lava flows indicate sub marine volcanic activity in deep portion of basin and pulling –catching the bottom of the basin. The location of the pillow lavas is probably near the outlet that forms continuous flood of lava, which after rapid cooling creates a typical structure of pillow lavas. In the study area, Pillow and massive lava flows are associated with pelagic sediment such as mudstone and radiolarian chert. The duration and time of oceanic processes can be concluded using biostratigraphy interpretation of the radiolarian chert (e.g. Bortolotti, *et al*., 2018). In this paper, we present result on geochemistry, petrology and biostratical dating of Ghaleh-Rigi pillow and massive lava flows associated with pelagic sediment. The goal of this paper is to use field data, petrographic analyses, and geochemical data, including REE and incompatible trace element data to identify different lithology and petrogenesis processes and possible tectonic environments of formation of this pillow and massive lava flows. The lithological and chemical signature of the mantle section can provide further insights on the tectonic setting where the magmatic rocks have formed.

Geological setting

The study area is located in the 28˚ 30' 41" northern latitude and 57˚ 29' 30" eastern longitude in the southern part of Nain-Baft suture and southern margin of Central Iran Micro-continent (CIM) block (Fig. 1b). Central Iran is comprised of metamorphic successions and plutonic suites (e.g. Chapedony and Posht-e-Badam metamorphic complexes: Haghipour, 1974; Nadimi, 2007; Precambrian plutonism: Berberian, 1981) and overlying Jurassic–Cretaceous and subordinate Paleogene covered formations.

Most importantly, Central Iran is surrounded by several ophiolitic domains (Nain–Baft, Sabzevar, Sistan; Fig. 1c) interpreted as minor oceanic seaways showing discontinuous oceanic crust emplacement and separated CIM from Eurasia (e.g. Stöcklin, 1974; Berberian & King, 1981; Knipper *et al*. 1986; Arvin & Robinson, 1994; Arvin & Shokri 1997; Shojaat *et al*. 2003). These domains correspond to the Upper Cretaceous to Paleocene-radiolarite and ophiolite ‘colored Melange’ of Gansser (1959) and to the inner Mesozoic oceans of McCall (1997). The Nain-Baft suture zone is located northward of the Mesozoic magmatic arc of the active margin of the Central Iranian block, reported in literature also as Sanandaj-Sirjan Zone. The Sanandaj-Sirjan Zone is a narrow zone of highly deformed rocks dominated by Mesozoic rocks, while the Paleozoic rocks are generally rare and restricted to the southeast in this zone. Several other relatively dismembered fragments of Neo-Tethyan ophiolite massifs occur along Sanandaj-

Sirjan zone on the western side of the CIM, (Shojaat *et al*., 2003). All massifs have tilted and fragmented highly into several tectonic slices with many strike–slip fault offsets. Several tectonic episodes are responsible for stacking and displacement of these tectonic slices. The ophiolitic rocks in the CIM are strongly imbricated and sheared by sub-vertical faults and shear zones (Alavi, 1994). The Nain–Baft ophiolite and the Sabzevar oceanic basins are thought to have opened during Late Cretaceous time and closed during Paleocene time (95–60 Ma; Davoudzadeh, 1972; Baroz *et al*., 1984; Sengör *et al*., 1988; Arvin & Robinson, 1994; Stampfli & Borel, 2002; Shojaat *et al.,* 2003). Few radiometric age constraints are available. Paleomagnetic data indicate that the CIM has rotated anti-clockwise during the Jurassic and opening of the Nain-Baft Ocean (Sengör, 1990). The Nain–Baft ophiolitic sutures are interpreted by several geologists as (i) the occurrence of a narrow oceanic basin like the Red Sea, between the Lut block and the active continental margin of the Iranian block known as Sanandaj–Sirjan Zone (e.g. Berberian & King, 1981); (ii) as a Cretaceous arc basin of Tethyan subduction (Desmons & Beccaluva, 1983; Hassanipak & Ghazi, 2000) and (iii) as Late Cretaceous Nain–Baft back arc basin (e.g. Arvin & Robinson, 1994; Shahabpour, 2005; Agard *et al*., 2006; Rahmani *et al*., 2007; Mehdipour Ghazi, 2008; Rahgoshay *et al*., 2008; Shafaii Moghadam *et al*., 2009; Pirnia *et al.,* 2010; Ghazi *et al*., 2010 a, b). (iv) the Nain-Baft basin underwent a counter-clockwise rotation in the Cenozoic, which displaced them in their present day position from an original northeastward location, and they firmed in arc-forearc setting was active in the Early Cretaceous (Pirnia *et al*., 2019).

Methods

Several assemblages of Radiolarian banded chert have been studied for biostratigraphy and the results are presented in Table 1 and 2. Samples were collected from all rock units and standard petrographic thin sections were prepared. Fifteen least-altered samples were selected for major and trace element geochemical analysis. Major elements in addition to Sc, Ba, and Ni were determined by inductively-coupled plasma atomic emission spectrometry (ICP-AES), whereas the rest of the trace elements including rare earth elements were analyzed by inductively-coupled plasma mass spectrometry (ICP-MS, ACME Analytical Laboratories Ltd, Vancouver, Canada performed all analyses).

Table 1. Compilation of chronological data, including extension of the radiolarian fauna, volcano-sedimentary magmatic series of the Ghaleh-Rigi area.

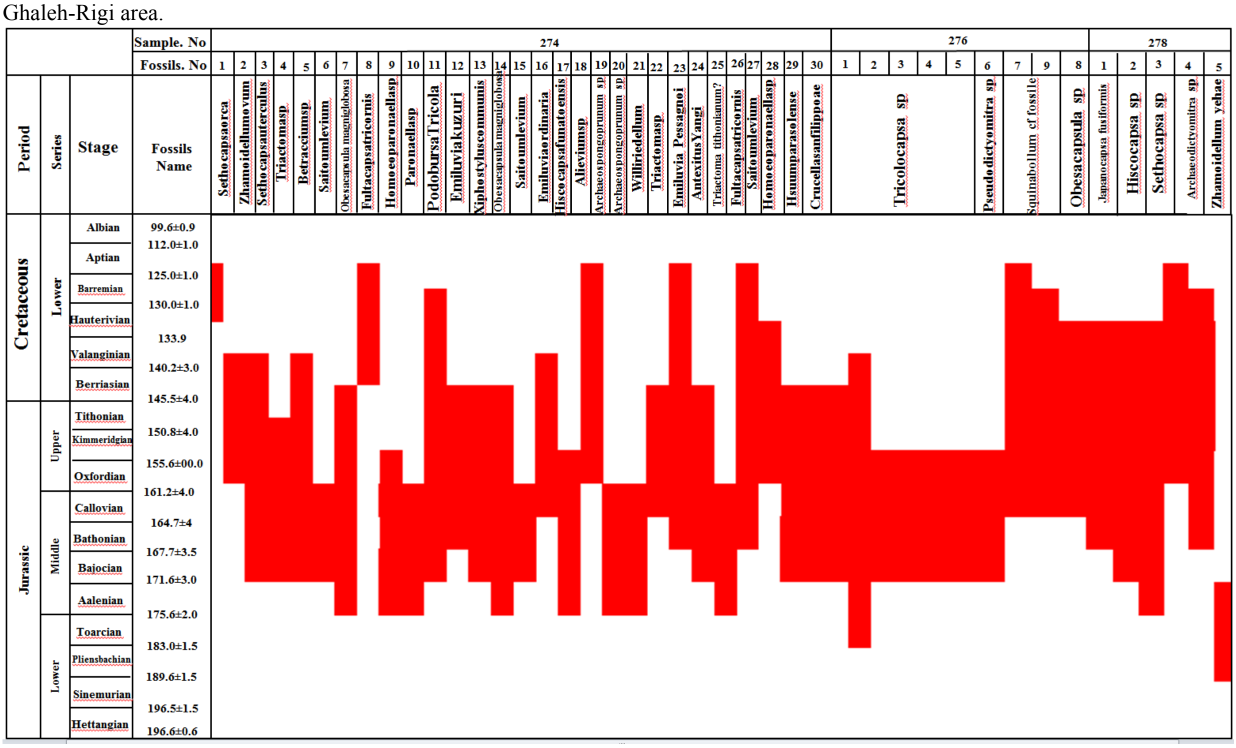

Table 2. Simultaneous time span of radiolarians with volcanic activity of the Ghaleh-Rigi area.

Sample No. and location	Age	Type of fossil
Gr-95-274 57˚28'59" E, 28˚30'17" N	Early Bajocian to Berriasian	Sethocapsa orca (Lukeneder *et al*., 2006), Zhamoidellum ovum (Baxter *et al.,* 2011), Sethocapsa uterculus (Matsuoka, 1992), Triactoma sp. (Goričan *et al*., 2006), Betraccium sp. (O'Dogherty *et al*., 2010), Saitoum levium. (Bejleri *et al.,* 2012), Fultacapsa tricornis. (Robini *at al*., 2010), Homoeoparonaella sp. (Goričan *et al.,* 2006), Paronaella sp (Goričan *et al.,* 2006), Podobursa Tricola (Foreman, 1973), Emiluvia kuzuri (Foreman, 1973), Xiphostylus communis (Yeh, 2011), Emiluvia ordinaria (Robini *et al.,* 2010), Hiscocapsa funatoensis (Yeh, 2011), Alievium sp. (Thurow, 1988), Archaeospongoprunum praeimlayi (Pessagno, 1982), Archaeospongoprunum sp. (Hattori *et al*.,1989), Williriedellum sp. (Matsuoka, 1983), Emiluvia Pessagnoi (Foreman, 1973), Antexitus Yangi (Yeh, 2009), Triactoma tithonianum? (Rust, 1985), Fultacapsa tricornis. (Robini *et al.,* 2010), Saitoum levium (Bejleri *et al.*, 2012), Hsuum parasolense (Pessagno *et al*., 1982), Crucella sanfilippoae (Pessagno, 1977)
Gr-95-274 57˚29'2" E, 28˚33'56" N	Collovian-Valanginian	Tricolocapsa sp (Goričan *et al.,* 2006), Pseudodictyomitra sp. (Babazadeh *et al.,* 2004), Squinabollum cf fossile (Squinabol, 1914), Obesacapsula sp. (Aita & Okada, 1986).
Gr-95-274 57˚28'52" E, 28˚30'02" N	Oxfordian – Valanginian	Japanocapsa fusiformis (Kozur, 1984), Hiscocapsa sp. (Pessagno, 1977), Sethocapsa sp (Goričan *et al*., 2006), Archaeodictyomitra sp (Goričan *et al*., 2006), Zhamoidellum yehae (Matsuoka, 1992).

It must be noted that all reported major element values were normalized to 100% on a volatile-free basis. Major and trace element concentrations of Ghaleh-Rigi micro gabbros and basalts are presented in Table 3.

Petrography

Geological map of the study area was prepared in the scale of 1:5000 (Fig. 2). Briefly, the most important rock units in this area from the oldest to the youngest are presented in the following.

Crystal Vitric Tuff Unit (CVTU)

This unit mainly consists of crystal vitric tuffs and is located in the east of Ghaleh-Rigi area (Fig. 2). It is located in lowest part of stratigraphic column and has been intruded by the Miocene dyke and other intrusive bodies (GSI, 2011). Two samples were picked up for petrography studies. The texture of these rocks is clastic and the main forming minerals are quartz, plagioclase, biotite and opaque minerals. Other minerals are, epidote, chlorite, zeolite, and calcite, all were formed in a glassy groundmass.

Lower Pelagic Sediment Unit

This unit is composed of pelagic sediment including mudstone, silty mudstone and chert associated with sporadic pillow and massive lava flows (minor) as intercalation (Fig. 2). Carbonate, clay, quartz, chlorite, epidote, zeolite, and opaque minerals are present. Chloritization and silicification are the most important alteration trends. This unit has copper, lead, zinc and gold massive sulfide mineralization (VMS).

Lower Volcano-Sedimentary Unit (LVSU)

This unit is mainly composed of basaltic pillow and massive lava flows associated with pelagic sediment (mudstone, silty mudstone, ribbon radiolarian chert) as intercalation. Volumetric, basaltic pillow and massive lava flows are the most important parts of this unit. A few samples were taken for the petrography and chemical analysis. There is a layer of pelagic deep-sea sediments including mudstones, silty mudstones, and a thin fine-grained sandstone with scattered basaltic flows associated with one meter thick micro gabbro.

Middle Pelagic Sediment Unit (MPSU)

This unit is located in the middle part of study area and completely is composed of pelagic sediment including cream to pale brown tuffaceous limestone, micritic limestone, mudstone, red to purple banded radiolarian chert, fine grain siltstone and shale (Fig. 2). Thin bedding and uniformity are the unique features of this unit. Samples were taken from this unit for bio-chronology and petrography (Gr-95-274). These rocks are very fine-grained and the textures are mainly microlithic and crystalline to cryptocrystalline. Carbonate crystals, which are mostly calcite, make up 65% of the rock. Other minerals are quartz, feldspar, pyroxene and volcanic fragments.

Upper pillow and Massive lava flows unit (UPMLFU)

Pillow and massive lava flows are the most important parts of this unit with pelagic sediments intercalation. Total compositions of these lavas are mainly basalt and some of them slightly tend to be andesitic basalt (Fig. 3a, b). The main textures of the rocks are porphyry (Fig. 3d), however, micro porphyry, intergranular, glomero-porphyritic, variolitic, and vesicular textures are also observed. Samples were taken from this unit for bio-chronology (Gr-95-276), petrography (Qr-95-89 and Gr-95-277) and chemical analysis (Qr-95-89).

Secondary minerals such as calcite, chlorite, zeolite and quartz have filled cavities in basalts. Plagioclase, pyroxene and opaque minerals observed in the matrix of microlith (Fig. 3d). Olivine, Plagioclase and clinopyroxene are the main minerals and Fe-oxides and titanite are the accessory minerals.

Table 3. Concentration of the major, trace and rare earth elements for the Ghaleh-Rigi basalts and gabbro.

	Pillow and massive lava								**Gabbro**						
Samples	**Dar.208**	**Dar.212**	**Qr.44**	**Qr.46**	**Qr.89**	**Qr.217**	**Gr.287**	**Gr.300**	**Qr.13**	**Qr.17**	**Qr.22**	**Qr.55**	**Qr.56**	**GR-316**	**DAR-203**
SiO_2	48.9	48.3	45.5	47.9	46.8	47.5	47.6	45.9	47.2	46.3	49	47	47.9	48.5	47.6
Al_2O_3	15.2	15.25	16.1	15.15	15.55	16.8	15.45	16.35	16.05	17.45	13.35	16.55	15.5	16.05	15.65
Fe_2O_3	10.75	10.5	9.4	9.26	9.57	9.21	11.1	10.5	11.95	10.9	10.35	9.79	10.7	11.3	10.55
CaO	9.88	10.65	12.85	12.9	12.2	11.3	10.6	11.6	11.8	11.25	9.05	11.1	10.5	9.4	10.9
MgO	6.73	7.14	7.1	7.15	7.24	6.04	7.69	8.11	6.43	6.77	8	6.9	6.88	7.69	7.35
Na_2O	3.47	3.25	2.37	2.59	2.15	3.27	3.46	2.84	2.56	3.15	3.26	2.73	2.91	3.26	2.62
K_2O	0.39	0.39	0.19	0.17	0.89	0.36	0.47	0.08	0.12	0.47	0.36	0.24	0.56	0.52	0.18
TiO_2	1.11	0.99	0.79	0.8	0.82	0.83	0.99	0.96	1.19	1.09	0.94	0.96	1.01	1.04	1.04
MnO	0.2	0.18	0.53	0.22	0.55	0.14	0.2	0.2	0.18	0.17	0.19	0.15	0.19	0.19	0.18
P_2O_5	0.09	0.08	0.05	0.08	0.09	0.08	0.08	0.09	0.11	0.08	0.07	0.06	0.08	0.09	0.08
Ba	80	110.5	102.5	49.6	536	130.5	117.5	124	31.7	141	347	116	102.5	205	73.8
Ce	6.8	6.7	5.6	6	5.5	5.3	6.7	6.6	8.3	6.6	7	5.8	6.6	7.4	6.7
Cr	110	220	280	260	240	150	220	290	100	140	220	200	160	110	220
Cs	0.33	0.46	0.2	0.06	0.83	0.48	2.22	2.65	0.39	0.69	0.54	0.61	1.81	0.67	0.26
Dy	4.38	3.77	3.33	3.23	3.18	3.01	3.89	3.94	4.32	3.66	3.98	3.38	3.94	4.07	4.05
Er	2.73	2.66	2.25	2.23	2.06	2	2.64	2.46	2.76	2.64	2.54	2.25	2.48	2.75	2.54
Eu	0.92	0.83	0.68	0.69	0.66	0.69	0.87	0.8	1.02	0.9	0.95	0.73	0.84	0.89	0.8
Ga	16.2	16.9	16.8	14.5	13.8	15.7	15.9	19.1	18.1	17	15.1	16.6	16.3	17.6	15.7
Gd	3.39	3.43	2.92	2.91	2.64	2.39	3.36	3.22	3.52	3.34	3.86	2.95	3.04	3.36	3.29
Hf	1.8	1.5	1.3	1.1	1.2	1.1	1.4	1.6	1.9	1.4	1.5	1.5	1.4	1.5	1.5
Ho	1	0.88	0.78	0.74	0.72	0.68	0.86	0.89	0.98	0.86	0.85	0.81	0.91	0.97	0.93
La	2.8	2.6	2.6	2.3	2.4	2.1	2.6	2.6	3.3	2.6	3.4	2.4	2.7	2.9	2.5
Lu	0.38	0.39	0.34	0.32	0.31	0.28	0.39	0.35	0.42	0.36	0.33	0.36	0.35	0.38	0.38
Nb	1.3	1.1	1	0.9	0.8	0.8	1.1	1.2	1.2	1.1	1.1	1	1	1	1.1
Nd	6.8	6.1	5.5	5.1	5	4.4	6.6	6.2	7.6	5.6	7	5.3	6.1	6.2	6.2
Pr	1.16	1.17	0.91	0.88	0.92	0.82	1.13	1.14	1.42	1.01	1.26	0.95	1.06	1.15	1.13
Rb	10	7.5	3.6	3.2	20.2	8.1	9.7	2.2	2.1	9.2	6.2	4.2	12.2	10.8	2.5
Sm	2.52	2.49	1.76	2.06	1.64	1.62	2.13	2.18	2.28	2.17	2.32	1.95	2	2.12	2.19
Sr	207	244	185	253	223	270	248	282	194	246	237	191	224	203	149
Ta	0.2	0.2	0.2	0.1	0.1	0.2	0.2	0.3	0.7	0.2	0.2	0.1	0.1	0.2	0.1
Tb	0.65	0.63	0.5	0.53	0.47	0.43	0.6	0.56	0.66	0.59	0.62	0.53	0.59	0.65	0.61
Th	0.32	0.27	0.32	0.28	0.28	0.2	0.29	0.39	0.32	0.25	0.26	0.23	0.34	0.33	0.32
Tm	0.44	0.41	0.34	0.3	0.34	0.33	0.4	0.36	0.41	0.35	0.36	0.35	0.39	0.43	0.4
U	0.08	0.09	0.21	0.16	0.09	0.08	0.08	0.12	0.11	0.07	0.14	0.07	0.09	0.09	0.11
V	353	339	315	287	281	268	317	309	382	324	321	298	331	333	302
Y	26.1	25.7	20.4	19.3	19.2	18	22.7	23.9	26.2	23.2	26.4	19.6	23.6	25	23.9
Yb	2.79	2.5	1.92	2.15	1.86	1.92	2.55	2.2	2.5	2.34	2.31	2	2.33	2.59	2.68
Zr	58	53	45	43	44	40	52	54	64	50	54	43	51	55	56
LOI	3.33	3.03	3.76	2.94	3.05	3.47	2.91	2.93	2.54	2.75	3.54	3.05	2.68	2.84	2.91
Total	100.08	99.82	98.7	99.22	99.02	99.06	100.61	99.63	100.15	100.44	98.19	98.58	98.95	100.93	99.11

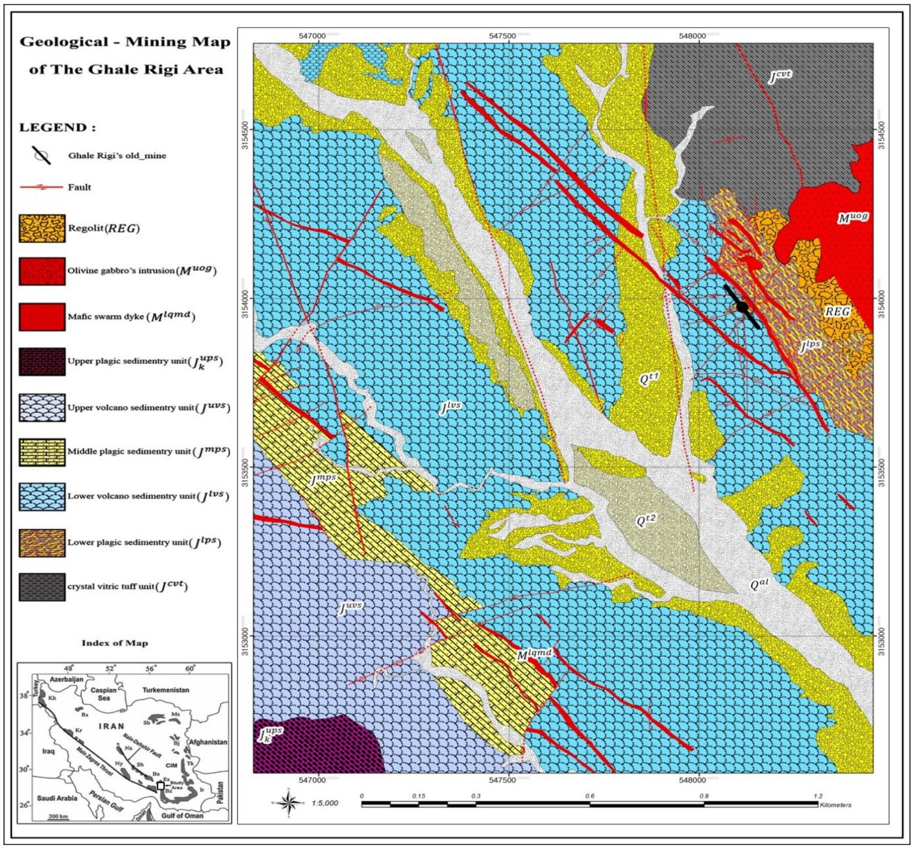

Figure 2. Simplified geological-mining map of Ghaleh–Rigi area showing the main rock units and mafic swarm dykes.

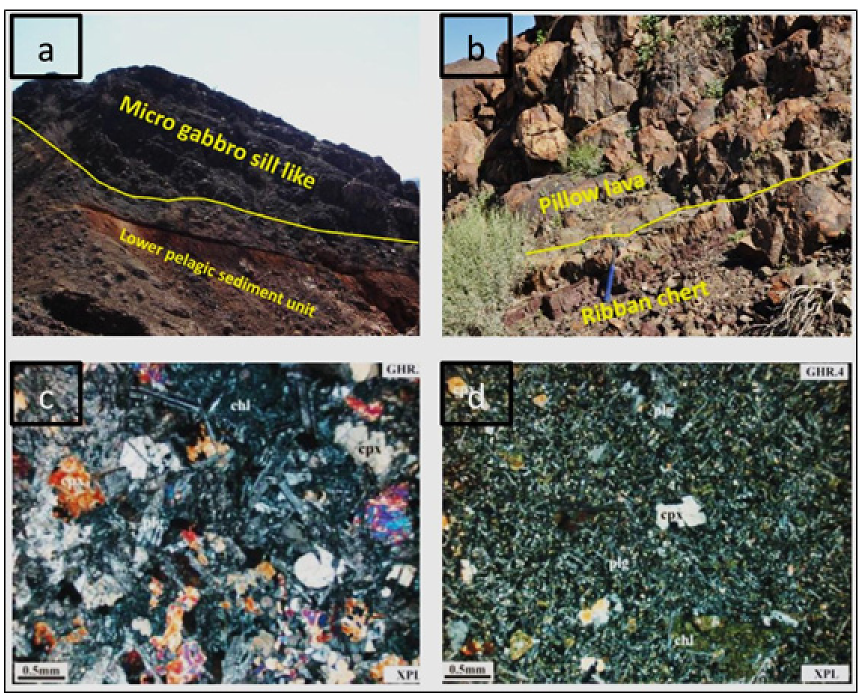

Figure 3. Field photographs and petrographical showing morphology of the pillow lava outcrops and mineralogy with texture at Ghaleh-Rigi area (a) Micro gabbro sill shape. (b) Pillow lavas associated with ribbon chert. (c) Gabbroic texture of micro gabbro. (d) Micro porphyry texture in basaltic pillow lava. cpx: Pyroxene, Pl: Plagioclase, Chl: Chlorite, Om: Opaque mineral.

Microscope investigations of clinopyroxene indicated that some of the clinopyroxene phenocrysts show reverse zonings. Carlsbad twinning developed in augite phenocrysts. Pyroxenes have partially changed to tremolite-actinolite and chlorite (Fig. 3d). Glomero-porphyritic texture can be observed with pyroxene minerals in some samples (Fig. 3d). Plagioclase occurs in two generation in the form of either phenocrysts or microlith. Generally it is altered to clay minerals and sericite and is replaced by calcite, chlorite and epidote. Olivine crystals in some samples have coarse anhedral to subhedral shapes, rounded and with abundant fractures (Fig. 3d).

Upper Pelagic Sediment Unit (UPSU)

This unit consists of pelagic sediments such as mudstone, magniferous thin bedded, red to purple radiolarian chert, siltstone and shale. This unit is mainly composed of elegant layers. Typical features of this unit are regular, coarse-grained layering with more than 100 meters thickness. This unit is mainly composed of tuffaceous limestone, shales, siltstone with inter bedded layers of radiolarian ribbon chert. The unit structurally was affected by normal and trike strike-slip faults. Samples were taken from this unit for bio-chronology (Gr-95-278).

Mafic Dyke Swarm Unit (MSDU)

This magmatic stage was observed in the form of very long and mafic parallel dyke swarm with northwest to southeast trend. The mafic swarm dykes have intruded old units such as pelagic sediment and pillow and massive lava flows with fine grandchild margin. These dykes indicate subophitic, porphyry, intergranular and microgranular textures in different parts. The main minerals are plagioclase, hornblende, feldspar, quartz and clinopyroxene. Plagioclase (50-55%) altered to chlorite, calcite, sericite and prehnite. The clinopyroxene minerals (augite-diopside) are subhedral to anhedral and altered into chlorite, tremolite and actinolite. Three samples were taken from this unit for petrography (Qr-95-2, Qr-95-3 and Gr-95-285) and chemical analysis (Qr-95-3 and Gr-95-285).

Gabbroic Intrusion Unit (GIU)

In general, this magmatic phase has intruded the older unit and caused contact metamorphism in its wall rock. The chemical composition of this intrusion is olivine gabbro to gabbro and belongs to upper Miocene (GSI, 2011). Based on petrographic study, micro gabbro show different textures including micro granular, inter granular, porphyry and ophitic. These rocks mainly consist of plagioclase, clinopyroxene, olivine (rare) and opaque minerals, whereas chlorite, actinolite, epidote, apatite, zeolite, titanite, sphene and calcite occur as secondary minerals. Some altered dolerite dykes also outcropped. The plagioclases formed in two generation. The anhedral pyroxenes are diopside –augitic in composition and are altered to chlorite and epidote (Fig. 3).

Biostratigraphy

Radiolarian assemblages play an important role in the biostratigraphy in regions with high tectonic intensity (Babazadeh *et al*., 2004). Several samples were examined in this study and among them; only in three samples identifiable radiolarian species have been found. The age of faunal assemblage in the Ghaleh-Rigi area is Early Bajocian (Middle Jurassic) to Berriasian (Early Cretaceous) as inferred from the radiolarian in the radiolarian banded cherts, pelagic limestone and radiolarian argillaceous cherts (Figs. 4, 5 and Table 1). Based on the results presented here from age studies on radiolarian fossils, there must be a sedimentary basin in the Middle Jurassic to Early Cretaceous in this area. Since sedimentation was associated with volcanic and intrusive activities, simultaneous time span of radiolarians with volcanic activity can be observed in this basin (Table 2).

Geochemistey

Major elements

According to geological and petrographic characteristics of igneous rocks in Ghaleh-Rigi, 15 samples were selected for major and trace element geochemical analysis. Geochemical studies represent values of SiO_2 45.5-49 wt.%, Al_2O_3 13.35-17.45 wt.%, MgO 6.04-8.11 wt. %, FeO (T) 5.24-6.84 wt.%, TiO_2 0.79-1.19 wt.%, P_2O_5 0.05-0.11 wt. %, Zr 40-54 ppm, Y 18.00-26.4 ppm, V 268-333 ppm and Cr 100-290 ppm (Table 3). Using the chemical classification diagram of LeBas et al., (1986) and Middlemost (1994) all samples plot in basalt or gabbro field (Fig. 6 a, b) and appear to be entirely subalkaline (Fig. 6c) and low-Ti basalts (Table 3; Fig. 6d).

Compatible and incompatible trace elements

Trace element concentration of studied samples is presented in Table 3.

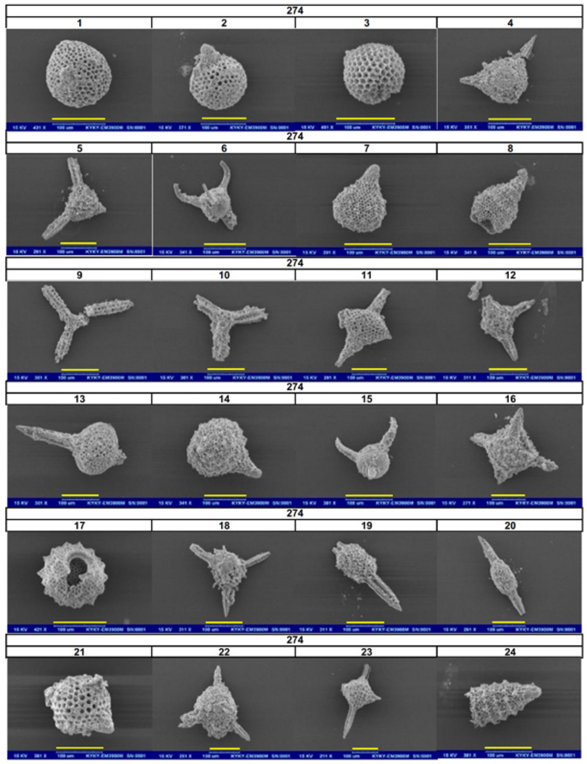

Figure 4. Scale bar = 50 µm1-Sethocapsa orca, 2-Zhamoidellum ovum, 3-Sethocapsa uterculus, 4-Triactoma sp.,5-Betraccium sp., 6-Saitoum levium,7-Obesacapsula magniglobosa, 8-Fultacapsa tricornis, 9-Homeoparanoella sp., 10-Paranaella sp.,11-Podobursa tricola, 12-Emiluvia kuzuri, 13-Xiphostylus communis,14-Obesacapsula magniglobosa, 15-Saitoum levium, 16-Emiluvia ordinaria, 17-Hiscocapsa funtoensis,18-Alievium,sp., 19-Archaeospongoprunum praeimlayi, 20-Archaeospongoprunum sp., 21-Williriedellum sp., 22-Triactoma sp., 23-Emiluvia pessagnoi, 24-Antexitus yangi.

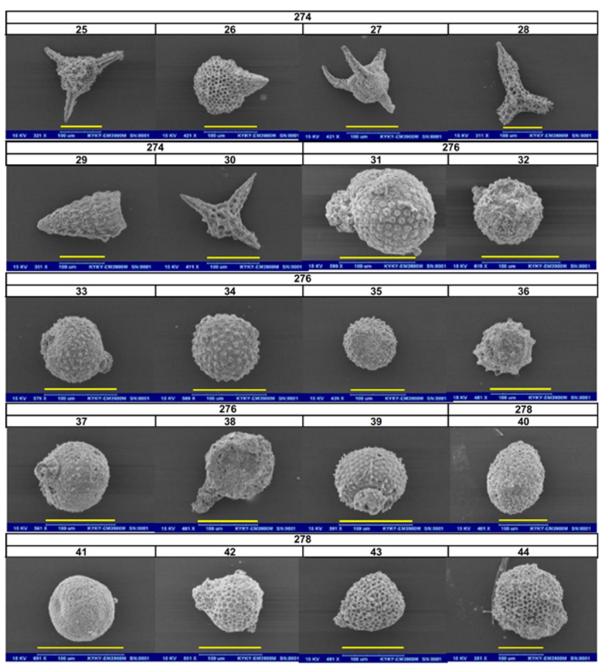

Figure 5. Triactoma tithonianum?, 26-Fultacapsa tricornis, 27-Saitum levium, 29-Homoeparanaella sp.29-Hsuum parasolense, 30-Crucella sanfilippoae, 31-35 Tricolocapsa sp., 36-Pseudodictyomitra sp.37- Squinabollum cf fossile, 38 -Obesacapsula sp. 39-Squinabollum cf fossile, 40-Japanocapsa fusiformis, 41-Hiscocapsa sp.,42-Sethocapsa sp.,43-Archaeodictyomitra sp.,44-Zhamoidellum yehae. Scale bar = 50 µm.

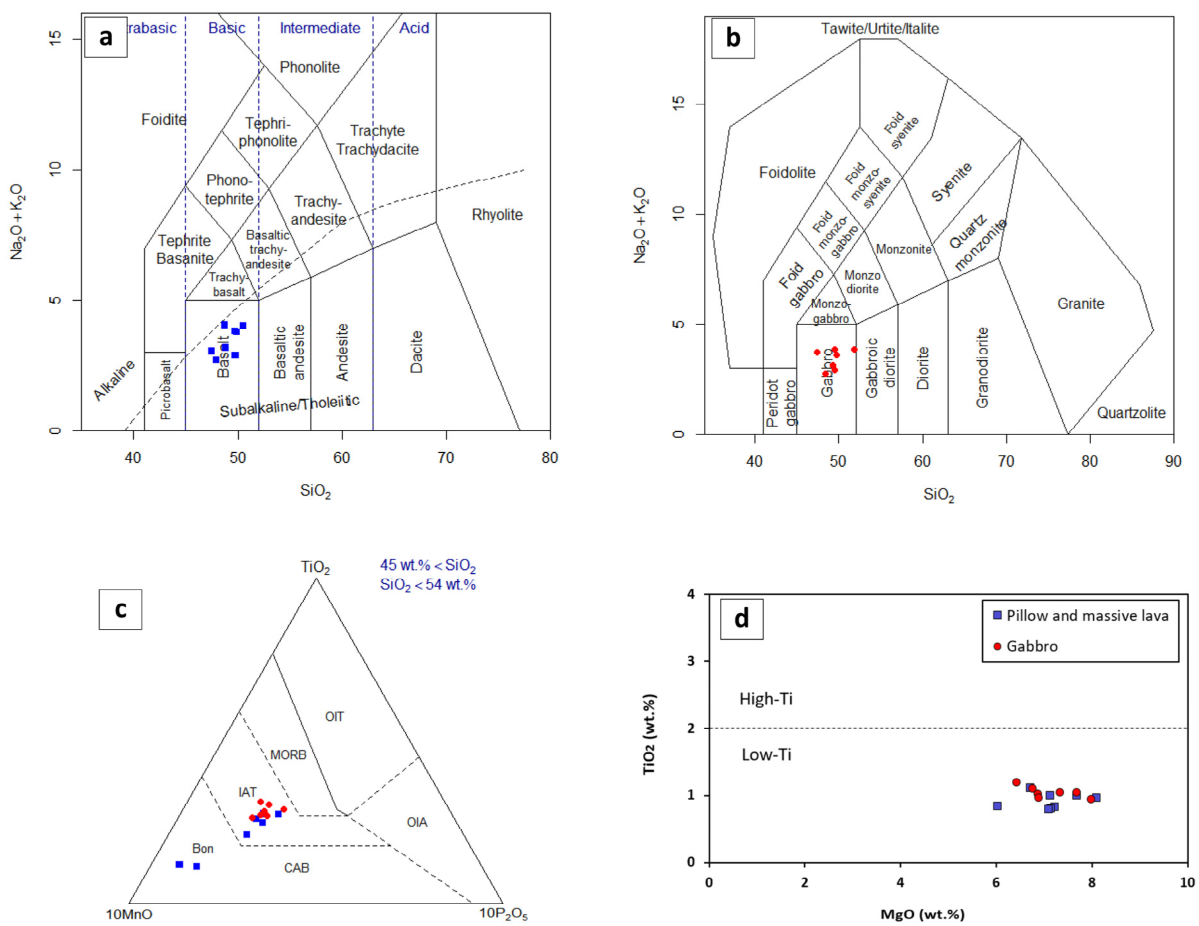

Figure 6. (a) Chemical classification of the basaltic rocks on Na_2O+K_2O/SiO_2 diagram (LeBas *et al.,* 1986). (b) Chemical classification of the gabbro samples on Na_2O+K_2O/SiO_2 diagram (Middlemost, 1994). (c) Most of samples show IAT environment on triangle diagram of $10MnO-TiO_2-10P_2O_5$ (Mullen, 1983). (d) All samples plot in low-Ti field on TiO_2 versus MgO diagram.

All samples display low Nb/Y values (0.04-0.05). Chondrite and primitive mantle normalized diagrams of trace elements abundances (Fig. 7) show enrichment of large-ion-lithophile elements (LILEs) with respect to the high field strength elements (HFSE), including Zr, Nb and Ti. Concentration of REE elements display near-flat pattern for the light rare earth elements (LREE) with respect to heavy rare earth elements (HREE).

These samples, besides the marked depletion in Th and Nb compared to other HFSE (e.g., Ti, P, Zr, and Y) Show similar geochemical features with Mid Ocean Ridge Basalt (MORB) and Island Arc Tholeite (IAT). As shown in Fig. 8, in the La/Nb and Ba/La ratios versus La diagrams, these samples all plot in the IAT field (Fig. 8).

Dicussion

Source features and variations

Gabbro and basaltic rocks display low TiO_2 (0.79-1.19 wt. %) (Fig. 6), with 0.8-1.2 ppm Nb and 40-64 ppm Zr concentration, suggesting similar mantle source and/or the same degrees of partial melting for their generation. Based on the Nb/Yb versus Th/Yb diagram the source region must be depleted and plot in the oceanic arc basalt field (Fig. 9a). Y/Nb values of the samples are also high (19.60-25) displaying similarities to depleted source (Pearce, 2008) (Fig. 9b).

REE ratios are sensitive to changes based on the presence of spinel or garnet in the mantle source.

The range of La/Sm versus Sm/Yb and La/Yb versus Dy/Yb based on non-modal batch melting of spinel garnet–lherzolite source of 50% PM and 50% MORB source composition (Göncüoglu *et al.*, 2010) show they may have formed by partial melting (around 10 percent) of a mixed spinel–garnet-bearing source (Fig. 10). This interpretation is based on a non-modal batch melting (Shaw, 1970) with distribution coefficients compiled from

McKenzie and O'Nions (1991), Kelemen *et al*. (1993), Bedard (1994) and Johnson (1998). Concentrations of depleted and primitive mantle were taken from McKenzie and O'Nions (1991). The samples show LILE enrichment, variable depletion in Th followed by depleted HFSE concentrations and distinct negative Nb anomalies (Th/Nb=0.23-035) (Fig. 7) which is a typical feature characterizing magmas related to subduction zones (Pearce, 1983; Peate *et al*., 1997; Gribble *et al*., 1998).

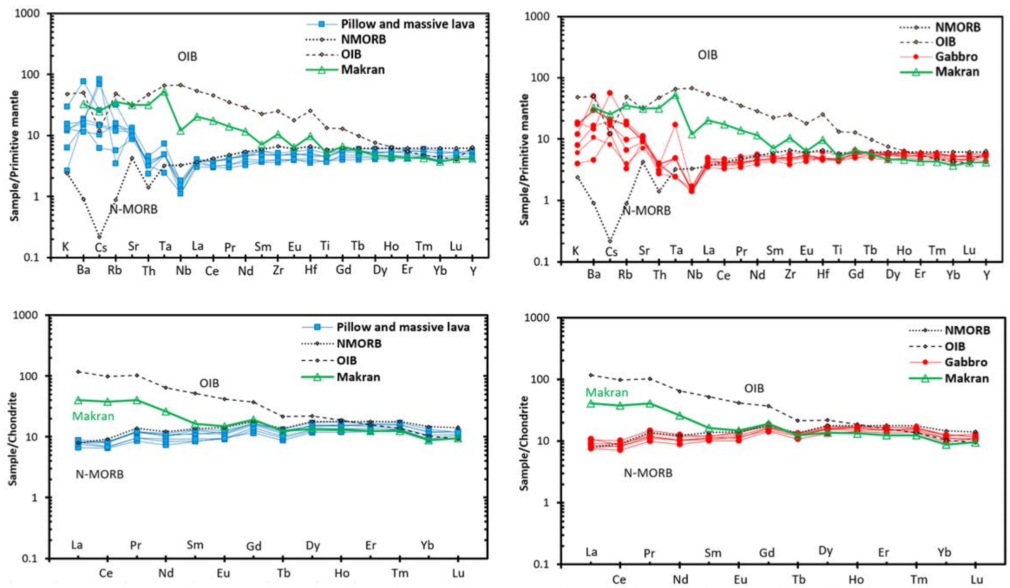

Figure 7. Trace element and REE variations of the Ghaleh-Rigi basalts and gabbros comparing with OIB, N-MORB and basaltic samples from Makran (Saadat & Stern, 2011). Normalization values from Sun and McDonough (1989).

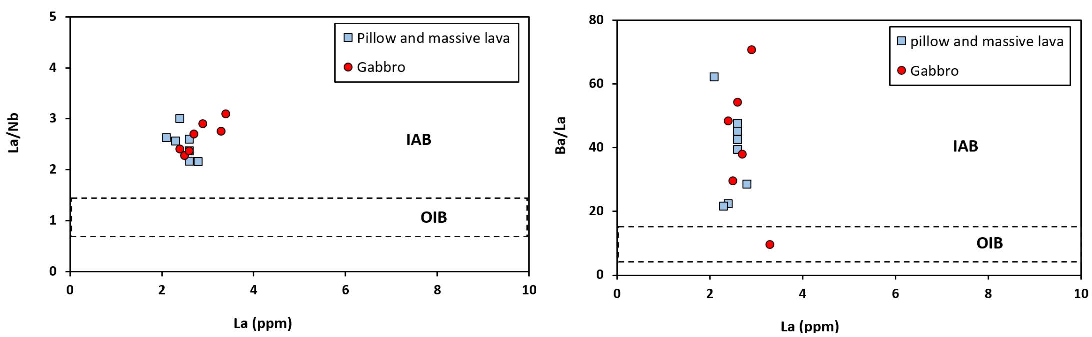

Figure 8. La/Nb and Ba/La ratios versus La concentration. The borderline of the field of OIB and MORB from Hickey-vargas *et al*. (1989).

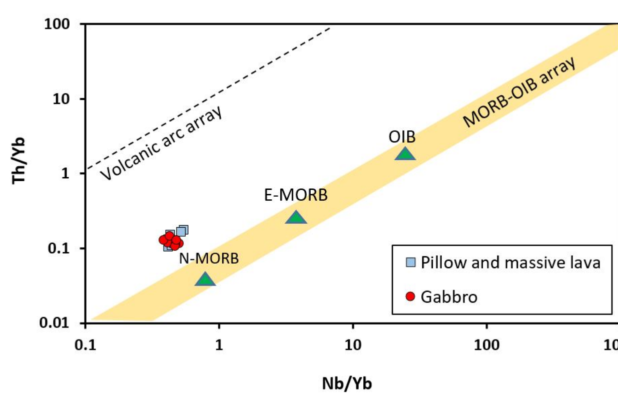

Figure 9. (a) Th/Yb versus Nb/Yb (Pearce, 2008). N-MORB and OIB compositions are from Sun and McDonough (1989).

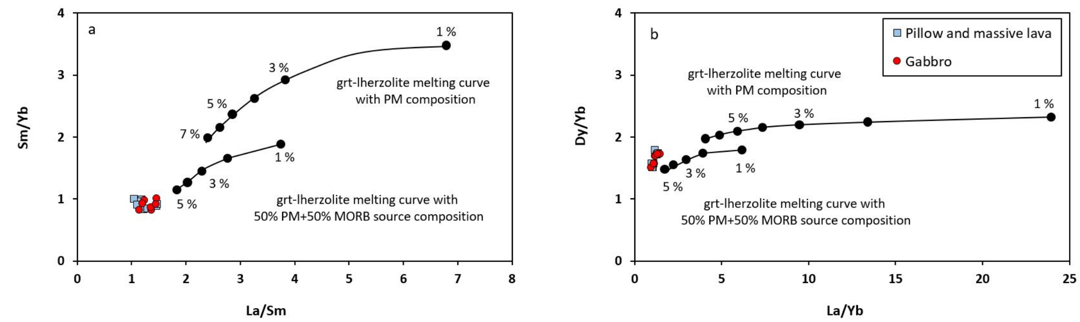

Figure 10. Variation of La/Sm–Sm/Yb and La/Yb–Dy/Yb for the Ghaleh-Rigi N-MORB-type Basalts and gabbros Melting paths based on non-modal batch melting of spinel garnet–lherzolite source of 50% PM and 50% MORB source composition. Garnet–lherzolite has a modal mineralogy of 0.60 oli + 0.20% opx + 0.14 cpx + 0.06 garnet melts in the proportions of 0.01 oli + 0.04 opx + 0.55 cpx + 0.40 grt (Haase *et al*., 1997). Spinel–garnet–lherzolite: 0.55 oli + 0.25 opx + 0.15 cpx + 0.014 grt, 0.03 spi that melts in the proportions of 0.05 oli + 0.05 opx + 0.30 cpx + 0.28 grt + 0.32 sp.

These chemical characteristics may have been inherited from Mesozoic subduction associated with the collision of the Arabian with the Eurasian plate.

These rocks are characterized by LREE-depleted patterns as indicated by low $(Ce/Yb)_N$ values (0.62–-0.85). According to Göncüoglu *et al*., (2010), these ratios resemble an N-MORB-like source. In addition, ratio of Y/Nb against Zr/Nb and Ce/Y against Zr/Nb also indicate all samples plot in N-MORB field (Fig. 11).

In general basaltic rocks rise fast and therefore they have usually minimum crustal contamination. Basalts that have experienced minimal or no crustal contamination characterize by low TiO_2/Yb ratios (Taylor & McLennan, 1995). Samples of the present study show low TiO_2/Yb ratio (0.37 to 0.48), low La/Nb (2.16-3) and La/Ta (4-24) indicating minimum crustal contamination (Hart *et al*., 1989; Saunders *et al*., 1992).

Tectono-magmatic evaluation

Any model of the tectonic setting and evolution of studied area must consider fundamental geochemical characteristics of their sequences, with specific regard to: (1) the geochemistry of the igneous rocks, (2) the nature and partial melting conditions of the mantle sources, and (3) the mutual relationships in terms of stratigraphy, tectonics and age of the different ophiolitic units. The petrological evidence with biostratigraphic data resulted in cognition of magmatic evolution of the Ghaleh-Rigi area.

All samples have tholeiitic basalts composition and small variation of TiO_2 and Nb contents and REE distribution reflect a uniform origin for their generation (Fig. 7). Indeed, the geochemical data presented in this study plot between volcanic arc and IAT fields in Ti/Zr discrimination diagram (Pearce & cann, 1973). They also fall mainly between volcanic arc and N-MORB fields in Triangular Y/15, La/10, Nb/8 diagram of Cabanis and Lecolle (1989). These geochemical characteristics indicate transitional environment between MORB and IAT (Saccani, 2018), indicating that they may have been generated in a back-arc basin (extensional regime) rather than in an island-arc setting (e.g. Volpe *et al*., 1990; Pearce *et al*., 1995; Gribble *et al*., 1998) (Fig. 12).

As pointed by Ghazi *et al*. (2011) for Nain–Baft ophiolitic belt petrological events, the following tectonic evolution can be suggested for Ghaleh-Rigi area:

(i) Based on bio-chronological investigation, the age of radiolarian faunal assemblage in the Ghaleh-Rigi area is Early Bajocian (Middle Jurassic) to Berriasian (Early Cretaceous). Radiolarian banded cherts and pelagic sediments associated with pillow and massive lava flows indicate sub marine volcanic activity in deep portion of oceanic basin during mid-Jurassic and Early Cretaceous in Ghaleh-Rigi area. (ii) Geochemical characteristic presented in this research shows a subduction signature followed by the release of slab-derived fluids/melts, which increased partial melting of the mantle wedge source. (iii) A slab roll-back occurred and resulted in intense mantle diapirism and generated moderate to low-Ti IAT magmas. (iv) Contemporaneous uprising of primitive asthenospheric mantle induced by continuous slab roll-back and generation of MORB sequences interlayered with MORB/IAT rocks (Fig. 13). The evolution of back arc mantle in the Ghaleh-Rigi area is similar to Nain Baft in Iran and evolution of the Northern Mariana back arc basin (Gribble *et al*., 1998) and Albanide–Hellenide ophiolites (Saccani *et al*., 2008).

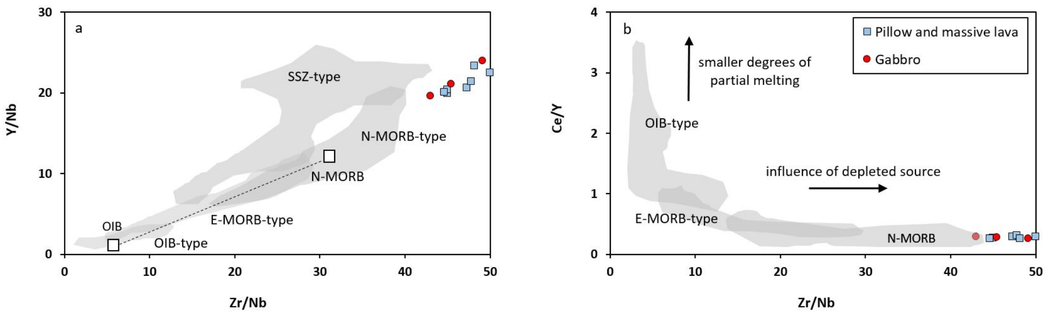

Figure 11. (a) Variation of Y/Nb against Zr/Nb for the studied samples. N-MORB and OIB compositions are from Sun and McDonough (1989); (b) Variation of Ce/Y against Zr/Nb for the studied samples. N-MORB and OIB compositions are from Sun and McDonough (1989).

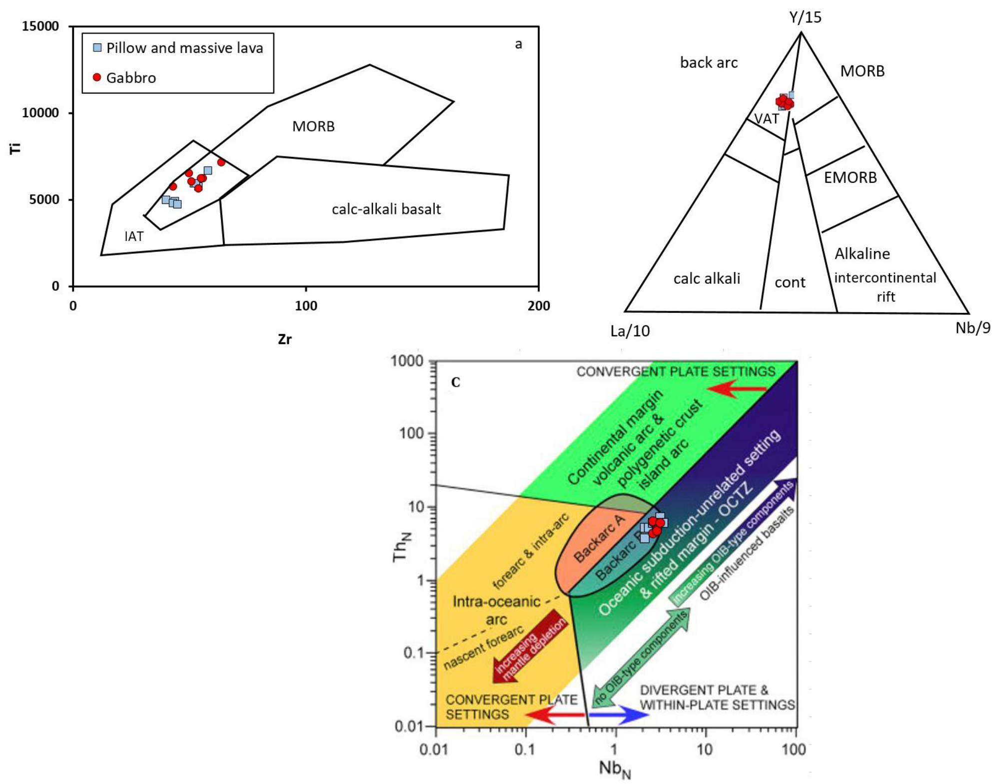

Figure 12. (a) Ti/Zr discrimination diagram (Pearce & cann, 1973). Samples of studied area plot between volcanic arc and IAT fields (b) Triangular Y/15, La/10, Nb/8 diagram of Cabanis and Lecolle (1989). Samples of studied area plot mainly between volcanic arc and N-MORB fields. (c) Samples plot in back arc setting in discrimination diagram of Saccani (2018).

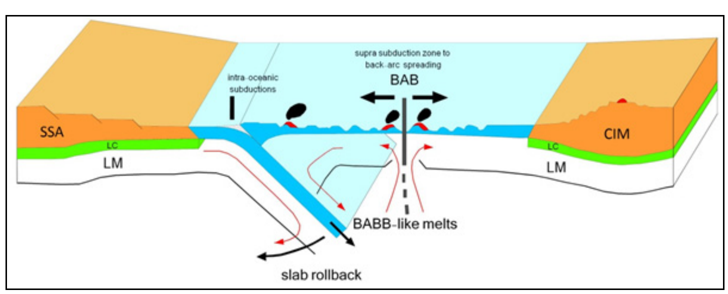

Figure 13. Sketch geodynamic model proposed for the oceanic domain between the margin of Sanandaj-Sirjan Arc (SSA) and the Margin of Central Iran Micro-continent (CIM) from Early Middle Jurassic to early Cretaceous times, from supra subduction zone (SSZ) to Back arc Spreading (Modified and after Hassig *et al*., 2015).

Summary and conclusions

This study focused on volcano-sedimentary series including oceanic lavas associated with pelagic sediments within the Ghaleh-Rigi area (between Nain –Baft and Makran ophiolitic belt), south west of Jiroft, south of Kerman province, southeast of Iran. Major and trace element analyses of mafic igneous rocks and a tailed bio-chronological investigation of the associated radiolarites (Radiolarian assemblages) from the Ghaleh-Rigi area led to the following conclusions.

The radiolarian cherts associated with volcanic rocks show the following ages: Early Bajocian to Berriasian (MPSU, gr-95-274), Collovian-Valanginian (UPMLFU, gr-95-276), Oxfordian-Valanginian (UPSU, gr-95-278).

Pillow and lava flows are mainly basalts in composition. In addition, minor andesite as well as micro gabbro are outcropped in this area. They show similar tholeiitic affinities and ages based on stratigraphic data (Early Middle Jurassic to Early Cretaceous).

The studied samples display mainly consistent multi-element patterns for HFSE and REE, indicating that the observed variations reflect primary igneous processes (Fig. 7). All rock types show depletion in Th and negative Nb anomalies. These rocks show transitional geochemical characteristics between MORB and IAT environment, indicating they may have been generated in a back-arc basin. These chemical characteristics may have been inherited from Mesozoic subduction associated with the collision of the Arabian with the Eurasian plate.

Based on partial melts of REE ratios, Ghaleh-Rigi basalts and gabbros show more than 10% partial melting of a mixed spinel–garnet-bearing source, which is composed of 50% PM and 50% MORB source.

Acknowledgments

This study is a part of the first author's Ph.D. dissertation at Ferdowsi University of Mashhad, Iran. The authors gratefully acknowledge Ahmad Rajabi for his contribution during the fieldwork and Cartography of maps. Special thanks go to Saeid Moatamed for taking micrographs of Radiolarian in Geological Survey and Mineral Exploration of Iran (GSI) applied research center, to Maliheh Ghoorchi for helping us to prepare some figures and two anonymous journal reviewers for their thoughtful and constructive comments that helped improve the paper.

References

Agard, P., Monie, P., Gerber, W., Omrani, J., Molinaro, M., Meyer, B., Labrousse, L., Vrielynck, B., Jolivet, L., Yamato, P., 2006. Transient, synobduction exhumation of Zagros blueschists inferred from P–T, deformation, time, and kinematic constraints: Implications for Neotethyan wedge dynamics. Journal of Geophysical Research Atmospheres, 111(B11):1–40.

Aita, Y., Okada, H., 1986. Radiolarians and calcareous nannofossils from the uppermost Jurassic and Lower Cretaceous strata of Japan and Tethyan regions. Micropaleontology, 32(2): 97–128.

Alavi, M., 1991. Sedimentary and structural characteristics of the Paleo– Tethys remnants in northeastern Iran, Geological Society of America Bulletin, 103: 983–992.

Alavi, M., 1994. Tectonics of Zagros orogenic belt of Iran, new data and interpretation. Tectonophysics, 229: 211–238.

Arvin, M. Robinson, P. T., 1994. The petrogenesis and tectonic setting of lavas from the Baft ophiolitic mélange, southwest of Kerman, Iran. Canadian Journal of Earth Sciences, 31: 824–834.

Arvin, M., Shokri, E., 1997. Genesis and eruptive environment of basalts from the Gogher ophiolitic mélange, southwest of Kerman, Iran. Ofioliti, 22: 175–182.

Babazadeh, S.A., Dewever, P., 2004. Radiolarian Cretaceous age of Soulabest radiolarites in ophiolite suite of eastern Iran. Bulletin of the Geological Society of France, 175(2): 121–129. (in French)

Bagheri, S. Stampfli, G. M., 2008. The Anarak, Jandaq and Posht–e–Badam metamorphic complexes in central Iran: New geological data, relationships and tectonic implications. Tectonophysics, 451:123–55.

Baroz, R., Macaudiere, J., Montigny, R., Noghreyan, H., Ohnenstetter, M., Rocci, G., 1984. Ophiolites and related formations in the central part of the Sabzevar range (Iran) and possible geotectonic reconstructions. Neues Jahrbuch für Geologie und Paläontologie, 168:358–388.

Baxter, A.T., Aitchison, J.C., Zyabrev, S.V., Ali, J.R., 2011. Upper Jurassic radiolarians from the Naga Ophiolite, Nagaland, northeast India. Gondwana Research, 20(2–3): 638–644.

Bedard, J.H., 1994. A procedure for calculating the equilibrium distribution of trace elements among the minerals of cumulate rocks, and the concentration of trace elements in the coexisting liquids. Chemical Geology, 118 (1–4):143–153.

Bejleri, A., Myfttu, M., Rrela, M., Bibera, A., 2012. The development of a database for radiolarian assemblages from the

Kalur Cherts of Albania. International Journal of Computer Science Issues 3, 9(2): 459–465.
Berberian, M., King, G.C.P., 1981. Toward a paleogeography and tectonic evolution of Iran. Canadian Journal of Earth Sciences, 18:210–265.
Bortolotti, V., Chiari, M., Goencueoglu, M. C., Principi, G., Saccani, E., Tekin, U. K., Tassinari, R., 2018. The Jurassic–Early Cretaceous basalt–chert association in the ophiolites of the Ankara Mélange, east of Ankara, Turkey: age and geochemistry. Geological Magazine, 155(2): 451–478.
Brocker, M., Fotoohi Rad, G. R., Thunissen, S., 2011. New time constraints for HP metamorphism and exhumation of mélange rocks from the Sistan suture zone, eastern Iran. An abstract paper in Symposium: Tectonic Crossroads: Evolving Orogens of Eurasia– Africa–Arabia. Turkey, Ankara.
Cabanis, B., Lecolle, M., 1989. The diagram La/10 – Y/15 – Nb/8: A tool for the discrimination of the volcanic series and in evidence of the mixture of crustal contamination. Account Rendus of the Academy of Sciences, 309(2) :2023–2029. (in French)
Davoudzadeh, M., 1972. Geology and Petrography of the Area North of Nain, Central Iran. Geological Survey of Iran, Report 14, 89 p.
Desmons, J., Beccaluva, L., 1983. Mid–oceanic ridge and island arc affinities in ophiolites from Iran: paleogeographic implication. Chemical Geology, 39: 39–63.
Dewey, J.F., Pitman, W.C., Ryan, W.B.F., Bonnin, J., 1973. Plate tectonics and the evolution of the alpine system, Geological Society of America Bulletin, 84(10): 3137–3180.
Dilek, Y., Furnes, H., 2019. Tethyan ophiolites and Tethyan seaways. Journal of the Geological Society, 176:899–912.
Elthon, D., 1979. High magnesia liquids as the parental magma for ocean floor basalts. Nature, 278: 514–518.
Foreman, H. P., 1973. Radiolaria from DSDP Leg 20. In Heezen, B. C, MacGregor, I. D., et al., Initial Reports, Deep Sea Drilling Project, Part II: Special Studies, 13:249–305.
Gansser, A., 1959. Asseralpine ophiolith problem. Eclogae Geologicae Helvetiae, 52(2):659–680.
Ghazi, J.M., Moazzen, M., Rahgoshay, M., Shafaii Moghadam, H., 2010a. Mineral chemical composition and geodynamic significance of peridotites from Nain ophiolite, central Iran. Journal of Geodynamics, 49: 261–270.
Ghazi, J.M., Moazzen, M., Rahgoshay, M., Shafaii Moghadam, H., 2011. The geodynamic setting of the Nain ophiolites, Central Iran: evidence from chromian spinels in the chromitites and associated rocks. Ofioliti, 36(1): 59–7.
Ghazi, J.M., Rahgoshay, M., Shafaii Moghadam, H., Moazzen, M., 2010b. Geochemistry of gabbroic pockets of a mantle sequence in the Nain ophiolite (Central Iran): constraints on petrogenesis and tectonic setting of the ophiolite. Journal of Mineralogy and Geochemistry, 187(1): 49–62.
Golonka, J., 2004. Plate tectonic evolution of the southern margin of Eurasia in the Mesozoic and Cenozoic. Tectonophysics, 38:235–273.
Göncüoglu, M.C., Sayit, K., Kagan Tekin, U., 2010. Oceanization of the northern Neotethys: Geochemical evidence from ophioliticmelange basalts within the İzmir– Ankara suture belt, NW Turkey. Lithos, 116:175–186.
Göncüoglu, M.C., Yaliniz, K., Tekin, U.K., 2006. Geochemistry, tectono–magmatic discrimination and radiolarian ages of basic extrusives within the IzmirAnkara Suture Belt (NW Turkey): time constraints. Ofioliti, 31(1): 25–38.
Goričan, S., Carter, E.S., Dumitrică, P., Whalen, P.A., Hori, R.S., De Wever, P., O'Dogherty, L., Matsuoka, A., Guex, J., 2006. Catalogue and systematics of Pliensbachian, Toarcian and Aalenian radiolarian genera and species. ZRC Publishing, 450 p.
Gribble, R.F., Stern, R.J., Newman, S., Bloomer, S.H., O'Hearn, T., 1998. Chemical and isotopic composition of lavas from the northern Mariana Trough; implications for magma genesis in back–arc basins. Journal of Petrology, 39:125–154.
GSI, 2011. Geologic map of the Ghaleh–Rigi Quadrangle, Geological Survey of Iran. Scale 1:25,000.
Haase, K.M., Stoffers, P., Garbe–Schönberg, C.D., 1997. The petrogenetic evolution of lavas 432 from Easter Island and neighbouring seamounts, near–ridge hotspot volcanoes in the SE 433 Pacific. Journal of Petrology, 38(6):785–813.
Haghipour, A., 1974. Geological survey of the Biabanak–Bafq region (Central Iran); Petrology and tectonics. Ph.D thesis, Grenoble Scientific and Medical University, 403p. (in French)
Hart, W.K., Wolde, Gabriel G., Walter, R.C., Mertzman, S.A., 1989. Basaltic volcanism in Ethiopia: constraints on continental rifting and mantle interactions. Journal of Geophysical Research, 94:7731–7748.
Hassanipak, A.A., Ghazi, A.M., 2000. Petrochemistry, ^{40}Ar–^{39}Ar ages and tectonics of the Nain Ophiolite, Central Iran. GSA Annual Meeting, Reno, pp. 237–238.
Hassig, M., Rolland, Y., Sosson, M., 2015. From seafloor spreading to obduction: Jurassic evolution of the northern branch of the Neotethys in the Northeastern Anatolian and lesser Caucasus regions. Geological Society London Special Publication, 428:41–60.
Hattori, I., Sakamoto, N., 1989. Geology and Jurassic radiolarians from manganese nodules of the Kanmuriyama–Kanakusadake area in the Nanjo Massif. Fukui prefecture, central japan. Bulletin of the Fukui Municipal Museum of Natural History, 36:25–79. (In Japanese with English abstract)

Hawkesworth, C.J., Hergt, J.M., Ellam, R.M., McDermott, F., 1991. Element fluxes associated with subduction related magmatism. Philosophical Transactions of the Royal Society, 335:393–405.

Hickey –Vargas, R., Roa, H.M., Escobar, L.L., Frey, F.A., 1989. Geochemical varitaions in Andean basaltic and silicic lavas from the Villarrica–Lanin volcanic chain (39.5 S): an evaluation of source heterogeneity, fractional crystallization and crustal assimilation. Contribution to mineralogy and Petrology, 103(3): 361–386.

Johnson, K.T.M., 1998. Experimental determination of partition coefficients for rare earth and high –field– strength elements between clinopyroxene, garnet and basaltic melt at high pressures. Contributions to Mineralogy and Petrology, 133:60– 68.

Kelemen, P.B., Shimizu, N., Dunn, T., 1993. Relative depletion of niobium in some arc magmas and the continental crust: partitioning of K, Nb, La and Ce during melt/rock reaction in the upper mantle. Earth and Planetary Science Letters, 120:111 – 134.

Knipper, A., Ricou, L. E., Dercourt, J., 1986. Ophiolite as indicator of the geodynamic evolution of the Tethyan Ocean. Tectonophysics 123, 213–240.

Kozur, H., 1984. New radiolarian taxa from the Triassic and Jurassic. Geologisch–Paläontologische Mitteilungen Innsbruck, 13(2):49–88.

LeBas, M.J., Le Maitre, R.W., Streckeisen, A., Zanettin, B., 1986. A chemical classification of volcanic rocks based on the total alkali–silica diagram. Journal of Petrology, 27(3): 745–750.

Lukeneder, A., Smrečková, M., 2005. An Early Cretaceous radiolarian assemblage: palaeoenvironmental and palaeoecological implications for the Northern Calcareous Alps (Barremian, Lunz Nappe, Lower Austria). 1st International Meeting on Correlation of Cretaceous Micro– and Macrofossils –Vienna. Series A for mineralogy and petrography, geology and paleontology, anthropology and prehistory, 23–57.

Marroni M., Göncüoğlu, C., Frassi, C., Sayit, K., Pandolfi, L., Ellero, A., Ottria, G., 2019. The Intra–Pontide ophiolites in Northern Turkey revisited: From birth to death of a Neotethyan oceanic domain. Geoscience Frontiers, in press, https://doi.org/10.1016/j.gsf.2019.05.010.

Matsuoka, A., 1983. Middle and Late Jurassic radiolarian biostratigraphy in the Sakawa and adjacent areas, Shikoku, Southwest Japan. Journal of Geoscience, Osaka City University, 26:1–48.

Matsuoka, A., 1992. Jurassic and Early Cretaceous radiolarians from ODP Leg 129, Sites 800 and 801, western Pacific ocean. Proceedings of the Ocean Drilling Program, Scientific results, College Station, TX, USA, 129:203–220.

McCall, G.J.H., 1997. The geotectonic history of the Makran and adjacent areas of southern Iran. Journal of Asian Science, 15:517–531.

McKenzie, D., O'Nions, R.K., 1991. Partial melt distributions from inversion of rare earth element concentr ations. Journal of Petrology, 32:1021 – 1091.

Mehdipour Ghazi, J., 2008. Geochemistry and petrology of mantle sequence in Nain ophiolite. M.Sc. Thesis. Shahid Beheshti University, Tehran, Iran, 225 p. (in Persian)

Middlemost, E.A.K., 1994. Naming Materials in the Magma/Igneous Rock System. Earth–Science Reviews, 37:215–244.

Moghadam, H.S., Whitechurch, H., Rahgoshay, M., Monsef, I., 2009. Significance of Nain–Baft ophiolitic belt (Iran): Short–lived, transtensional Cretaceous back–arc oceanic basins over the Tethyan subduction zone. Comptes Rendus Geoscience, 341(12), pp.1016–1028.

Moores, E. M., Kellogg, L. H., Dilek, Y., 2000. Tethyan ophiolites, mantle convection, and tectonic `historical contingency': a resolution of the `ophiolite conundrum. In: Dilek, Y., Moores, E. M., Elthon, D. and Nicolas, A. (eds) Ophiolites and Oceanic Crust: New Insights from Field Studies and the Ocean Drilling Program. Geological Society of America, Special Papers, 349:3–12.

Mullen, E.D., 1983. $MnO/TiO_2/P_2O_5$: A Minor Element Discriminant for Basaltic Rocks of Oceanic Environments and Its Implications for Petrogenesis. Earth and Planetary Science Letters, 62:53–62.

Nadimi, A., 2007. Evolution of the Central Iranian basement. Gondwana Research, 12:324–33.

O'Dogherty, L., Carter, E.S., Goričan, Š. and Dumitrica, P., 2010. Triassic radiolarian biostratigraphy. Geological Society, London, Special Publications, 334(1):163–200.

Pearce, J.A., 1983. Role of the sub–continental lithosphere in magma genesis at active continental margins. In: Hawkesworth, C.J., Norry, M.J. (Eds.), Continental Basalts and Mantle Xenoliths, 230–249.

Pearce, J.A., 2008. Geochemical fingerprinting of oceanic basalts with applications to ophiolite classification and the search for Archean oceanic crust. Lithos, 100:14–48.

Pearce, J.A., Cann, J.R., 1973. Tectonic setting of basic volcanic rocks determined using trace element analyses. Earth and Planetary Science Letters, 19:290–300.

Pearce, J.A., Peate, D.W., 1995. Tectonic implications of the composition of volcanic arc magmas. Annual Review of Earth and Planetary Sciences, 23:251– 285.

Peate, D.W., Pearce, J.A., Hawkesworth, C.J., Colley, H., Edwards, C.M.H., Hirose, K., 1997. Geochemical variations in Vanuatu arc lavas: the role of subducted material and a variable wedge composition. Journal of Petrology, 38:1331–

1358.
Pessagno, E. A., 1977. Upper Jurassic Radiolaria and Radiolarian Biostratigraphy of the California coast range. Micropaleontology, 23(1):117–134.
Pessagno, E. A., Whalen, P., 1982. A Middle Jurassic (upper Bajocian) Radiolarian Assemblage from Snowshoe Formation, east–central Oregon. British Columbia Micropaleonotology, 28(2):11–189.
Pirnia, T., Arai, S., Torabi, G., 2010. Post–deformational impregnation of depleted MORB in Nain lherzolite (Central Iran). Journal of Mineralogical and Petrological Sciences, 105:74–79.
Pirnia, T., Saccani, E., Torabi, G., Chiari, M., Goričan, S., Barbero, E., 2019. Cretaceous tectonic evolution of the Neo–Tethys in Central Iran: Evidence from petrology and age of the Nain–Ashin ophiolitic basalts. Geoscience Frontiers. In press. https://doi.org/10.1016/j.gsf.2019.02.008.
Rahgoshay, M., Ghazi, M.J., Shafaii Moghadam, H., 2008. Geochemistry and petrology of mantle sequence in Nain ophiolite. Geosciences Scientific Quarterly Journal, 71:31–44. (in Persian)
Rahmani, F., Noghreyan, M., Khalili, M., 2007. Geochemistry of sheeted dikes in the Nain ophiolite (Central Iran). Ofioliti, 32(2): 119–129.
Richards, J.P., 2014. Tectonic, Magmatic and Metallognic Evolution of the Tethyan Orogen: From Subduction to Collision. Ore Geology Reviews, 70:323–345.
Robertson, A.H.F., 2007. Overview of tectonic settings related to the rifting and opening of Mesozoic ocean basins in the Eastern Tethys: Oman, Himalayas and Eastern Mediterranean regions. In: Karner, G., Manatschal, G., Pinheiro, L. (Eds.), Geological Society, London Special Publication, 282: 325–389.
Robini, C. Gorican, S., Guillocheaui, F., Razin, P., Dromart, G. Mosaffa, H., 2010. Mesozoic deep–water carbonate deposits from the southern Tethyan passive margin in Iran (Pichakun nappes, Neyriz area): biostratigraphy, facies sedimentology and sequence stratigraphy. Geological Society, London, Special Publications, 330 (1):179–210.
Saadat, S., Stern, C.R., 2011. Petrochemistry and genesis of olivine basalts from small monogenetic parasitic cones of Bazman stratovolcano, Makran arc, southeastern Iran. Lithos, 125:609–617.
Saccani, E., 2018. A new method of discriminating different types of post–Archean ophiolitic basalts and their tectonic significance using Th–Nb and Ce–Dy–Yb systematics. Geoscience Frontiers, 6(4):481–501.
Saccani, E., Allahyari, K., Beccaluva, L., Bianchini, G., 2012. Geochemistry and petrology of the Kermanshah ophiolites (Iran): implication for the interaction between passive rifting, oceanic accretion, and plume–components in the Southern Neo–Tethys Ocean. Gondwana Research 24, 1:392–411.
Saccani, E., Photiades, A., Beccaluva, L., 2008. Petrogenesis and tectonic significance of Jurassic IAT magma types in the Hellenide ophiolites as deduced from the Rhodiani ophiolites (Pelagonian zone, Greece). Lithos, 104(1–4): 71–84.
Saunders, A.D., Storey, M., Kent, R.W., Norry, M.J., 1992. Consequences of plume– lithosphere interactions. In: Storey, B.C., Alabaster, T., Pankhurst, R.J. (Eds.), Magmatism and the Causes of Continental Break–up: Geological Society, London, Special Publications, 68: 41–60.
Sengor, A.M.C., Kidd, W.S.F., 1979. The post–collisional tectonics of the Turkish–Iranian Plateau and a comparison with Tibet: Tectonophysics, 55(3–4):361–376.
Shafaii Moghadam, H., Stern, R.J., 2011. Geodynamic evolution of Upper Cretaceous Zagros ophiolites: formation of oceanic lithosphere above a nascent subduction zone. Geological Magazine ,148: 762–801.
Shafaii Moghadam, H., Stern, R.J., Rahgoshay, M., 2010. The Dehshir ophiolite (central Iran): Geochemical constraints on the origin and evolution of the Inner Zagros ophiolite belt. Geological Society America Bulletin, 122:1516–1547.
Shahabpour, J., 2005. Tectonic evolution of the orogenic belt in the region located between Kerman and Neyriz. Journal of Asian Earth Sciences, 24:405–417.
Shaw, D.M., 1970. Trace element fractionation during anatexis. Geochimica et Cosmochimica Acta, 34(2):237–243.
Shojaat, B., Hassanipak, A.A., Mobasher, K., Ghazi, A.M., 2003. Petrology, geochemistry and tectonics of the Sabzevar ophiolite, North Central Iran. Journal of Asian Earth Science, 21:1053–1067.
Stampfli, G.M., Borel, G.D., 2002. A plate tectonic model for the Paleozoic and Mesozoic constrained by dynamic plate boundaries and restored synthetic oceanic isochrones. Earth and Planetary Science Letters, 196:17–3.
Stampfli, G.M., Borel, G.D., Cavazza, W., Mosar, J., Ziegler, P.A., 2001. Palaeotectonic and palaeo geographic evolution of the western Tethys and Peri–Tethyan domain (IGCP Project 369). Episodes 24, 4:222–227.
Stocklin, J., 1968. Structural history and tectonics of Iran: A review: The American Association of Petroleum Geologists Bulletinm, 52:1229–1258.
Stocklin, J., 1974. Possible ancient continental margin in Iran. In: Burke, C. A. and Drake, C. L. (Eds.): The Geology of Continental Margins. Springer–Verlag, New York, 873–877.
Sun, S.S., McDonough, W.F., 1989. Chemical and isotopic systematics of ocean basalts: Implications for mantle composition and processes. In: Saunders, A.D., Norry, M.J. (Eds.), Geological Society of London Special Publication, 42: 313–34.

Takin, M. 1972. Iranian geology and continental drift in the Middle East. Nature, 235:147–150.

Taylor, S.R., McLennan, S.M., 1995. The Geochemical Evolution of Continental Crust. Reviews of Geophysics, 33:241–265.

Thurow, J.W., 1988. Cretaceous radiolarians of the North Atlantic Ocean: ODP Leg 103 (sites 638, 640, and 641) and DSDP legs 93 (Site 603) and 47B (Site 398). In: Boillot, G; Winterer, EL; et al. (eds.), Proceedings of the Ocean Drilling Program, Scientific Results, College Station, TX (Ocean Drilling Program), 103:379–418.

Volpe, A.M., Macdougall, J.D., Lugmair, G.W., Hawkins, J.W., Lonsdale, P., 1990. Fine–sale isotopic variation inMariana Trough basalts: evidence for heterogeneity and a recycled component in backarc basin mantle. Earth and Planetary Science Letters, 100:251–264.

Weber–Diefenbach, K., Davoudzadeh, M., Alavi Tehrani, N., Lench, G., 1986. Paleozoic ophiolites in Iran, Geology, geochemistry and geodynamic implication. Ofioliti, 11:305–338.

Yeh, K., 2011. A Middle Jurassic (Upper Bajocian) Radiolarian Assemblage from Snowshoe Formation, East–Central Oregon. Collection and research, 24:1–77.

Zhang, C., Manheim, F.T., Hinde, J., Grossman, J.N., 2005. Statistical characterization of a large geochemical database and effect of sample size. Applied Geochemistry, 20:1857–1874.